A preliminary study of the causal structure in fully developed near-wall turbulence

By X. San Liang† AND A. Lozano-Durán

Despite the huge amount of information provided by direct numerical simulations of turbulent flows, the underlying dynamics remains elusive even in the simplest and most canonical configurations. An important observation in nonlinear dynamical systems in general, and turbulent flows in particular, is that, as time goes by, the correlation between two events may be lost and/or re-emerge. This raises a crucial issue, i.e., causality, which has been overlooked in turbulence research. Using a newly developed rigorous causality analysis, we have examined the causal structure between the streaks and rolls in the logarithmic layer of a plane turbulent channel flow. The velocity streaks are represented by the first proper orthogonal modes of the streamwise velocity, while the rolls are defined by the wall-normal and spanwise velocities. It is found that the streak-roll regeneration cycle may be seen as a combination of two subcycles: one between the collection of unbroken streaks and the wall-normal velocity, another between the spanwise velocity and the meandering streaks. Both are mutually causal. These subcycles are connected through the interaction between the wall-normal and spanwise velocities.

1. Introduction

Turbulence is an important nonlinear dynamical phenomenon and one of the most difficult problems in classical physics; however, it has not been systematically investigated from the point of view of causality, which makes a crucial issue for nonlinear systems. One reason may be attribted to the lack of appropriate research tools. To date, the only attempt to study causality in turbulence is the conference paper by Tissot et al. (2014), where the so-called Granger causality is used (Granger 1969). In this study, we will employ a newly developed rigorous causality analysis to investigate the interaction between the well-observed rolls and streaks in the logarithmic layer of fully developed wall-bounded turbulence.

Streamwise rolls and streaks are ubiquitous in wall-shear flows. Ever since the experiment by Klebanoff et al. (1962) and the discovery of sublayer streaks and ejections by Kline et al. (1967), among others, the roll-streak structure has attracted enormous interest within the fluid mechanics community. The spatially and temporally varying structure is generally believed to play an important role in maintaining the turbulence in shear flows (e.g., Kim et al. 1971; Jiménez & Moin 1991; Hamilton et al. 1995; Waleffe 1997; Schoppa & Hussain 2002), and to serve as a vehicle carrying the turbulence (cf. Jiménez 2013). Most analyses focus on the buffer layer where the streaks and rolls (vortices in this case) are essentially one-scale objects and the analysis is simpler. Farther from the wall, streaks and rolls persist but their internal Reynolds numbers are higher, making their characterization and understanding a more challenging task.

We will center our study in the logarithmic layer of a turbulent channel flow. A

† Nanjing Institute of Meteorology, China

paramount question that follows is how rolls and streaks are generated in a self-sustaining way. Although it is widely agreed that in both the buffer and logarithmic layers the streaks and rolls are involved in a regeneration cycle, many different mechanisms have been proposed derived from simplified scenarios. In the buffer layer, it has been hypothesized that streamwise vortices near the wall may collect the fluid from the inner region where the flow is very slow and organize it into filaments (see Panton 2001); streaks may be created by the wall-normal advection of the streamwise velocity by the vortices (cf. Jiménez 2013). The streaks, on the other hand, may spawn formation of the rolls through losing stability (Schoppa & Hussain 2002); and the instability includes the normal hydrodynamic instability, stochastic structural instability (Farrell & Ioannou 2012), among others. A similar but more disorganized scenario is believed to take place in the logarithmic layer, with the Orr's mechanism playing an important role in the formation of the streaks (Jiménez 2015).

The different mechanisms, each capable of leading to the turbulence structure as expected, are rooted in theoretical or conceptual arguments. Whether nature picks one, more than one, or none, is in fact unclear. In the following, the causal structure analysis is expected to help in clarifying the drives and consequences. Our study is completely data-driven and independent of conceptual models.

The paper is organized as follows. First, we give a brief introduction of the state-of-the-art of causality analysis (Section 2), and then the dataset (Section 3). The streak-roll interaction and the resulting causal structure are presented in Section 4. Finally, the study is summarized in Section 5.

2. Quantitative causality analysis

Causal inference is an important subject in different scientific disciplines. It is also a very challenging problem. During the past decades, many empirical or half-empirical formalisms have been proposed for specific purposes in their respective contexts (for references, see Liang 2014). Recently, it is found that causality, which traditionally has been taken as a concept in statistics (e.g., Granger 1969), is actually a real physical notion, and, therefore, causality analysis can be put on a rigorous footing, rather than formulated as a statistical hypothesis test (like the renowned Granger causality test). With this faith, Liang (2014) was able to establish a rigorous and quantitative formalism to address the causal inference challenge (cf. Liang 2014, hereafter L14; Liang 2015).

In the L14 formalism, causality is measured as the rate of information flow or transfer from one event to another. The logical association of information flow with causality has been gradually and universally recognized after more than three decades of research. For a historical account, see Liang (2016). As a start, consider a stochastic system in the form

$$\frac{dX_1}{dt} = F_1(X_1, X_2, t) + b_{11}\dot{W}_1 + b_{12}\dot{W}_2, \tag{2.1}$$

$$\frac{dX_2}{dt} = F_2(X_1, X_2, t) + b_{21}\dot{W}_1 + b_{22}\dot{W}_2, \tag{2.2}$$

where $\dot{W}_1$ and $\dot{W}_2$ are independent white noises, and F_1 and F_2 arbitrary differentiable nonlinear functions of (X_1, X_2). With respect to the system, the major results can be summarized in the following theorems.

THEOREM 2.1. (Liang, 2008)

For the dynamical system Eqs. (2.1)-(2.2), the rate of information (in terms of entropy transfer) flowing from X_2 to X_1 is

$$T_{2\to 1} = -E\left[\frac{1}{\rho_1}\frac{\partial(F_1\rho_1)}{\partial x_1}\right] + \frac{1}{2}E\left[\frac{1}{\rho_1}\frac{\partial^2(b_{11}^2 + b_{12}^2)\rho_1}{\partial x_1^2}\right], \tag{2.3}$$

where E stands for mathematical expectation, and $\rho_1 = \rho_1(x_1)$ is the marginal probability density of X_1.

THEOREM 2.2. Principle of nil causality (Liang, 2008)
If in the system Eqs. (2.1)-(2.2), F_1, b_{11}, and b_{12} are independent of X_2, then $T_{2\to 1} = 0$.

In causality analysis, perhaps the only observational fact that can be stated in a quantitative way is the following nil causality principle:

If the evolution of a variable, say X_1, is independent of another one, X_2, then the causality from X_2 to X_1 is zero.

However, it has been shown that the previous empirical causality analyses, including the Granger causality, fail to verify this principle in a wide range of situations (for references, see Liang 2016). In the L14 formalism, however, this is stated in a proven theorem.

In many practical applications, Eq. (2.3) becomes infeasible to evaluate, even if the equations of motion of the system in question are well known. This is the case of turbulent flows involving millions of degrees of freedom. However, given two time series, the information flows can be approximated through maximum likelihood estimation.

THEOREM 2.3. (Liang, 2014)
Given time series X_1 and X_2, with a linear model the maximum likelihood estimator (MLE) of the rate of information flowing from X_2 to X_1 is

$$T_{2\to 1} = \frac{C_{11}C_{12}C_{2,d1} - C_{12}^2 C_{1,d1}}{C_{11}^2 C_{22} - C_{11}C_{12}^2}. \tag{2.4}$$

Here $\mathbf{C} = (C_{ij})$ is the sample covariance matrix between time series X_1 and X_2, and $C_{i,dj}$ the sample covariance between X_i and a series derived from X_j using Euler forward differencing scheme: $\dot{X}_{j,n} = (X_{j,n+1} - X_{j,n})/\Delta t$. The units are in nats per unit time.

Note that in Eq. (2.4) T is actually the MLE of the information flow rate and, strictly, should bear a hat. The abuse of notation here should not cause confusion since we will rely on Eq. (2.4) only to infer causality henceforth. Specifically, Eq. (2.4) will be used to quantify the causality from X_2 to X_1: When $|T_{2\to 1}| > 0$, X_2 is the cause of X_1; if $T_{2\to 1} = 0$, X_2 is not causal.

Note that Eq. (2.4) demonstrates explicitly that causation implies correlation, but not vice versa, resolving the long-standing philosophical debate over causation versus correlation (Liang 2014).

The formalism has proven successful in many well-known, low-dimensional chaotic systems, where the causal relation between time series can be accurately recovered using the concise formula in Eq. (2.4). The power of Eq. (2.4) has also been validated in many remarkably successful real-world applications, among which are the clarification of the causality between CO_2 and global warming (Stips et al. 2016), and the unraveling of a period of unusual causal relation between IBM and GE from the time series of their respective stock prices (Liang 2015).

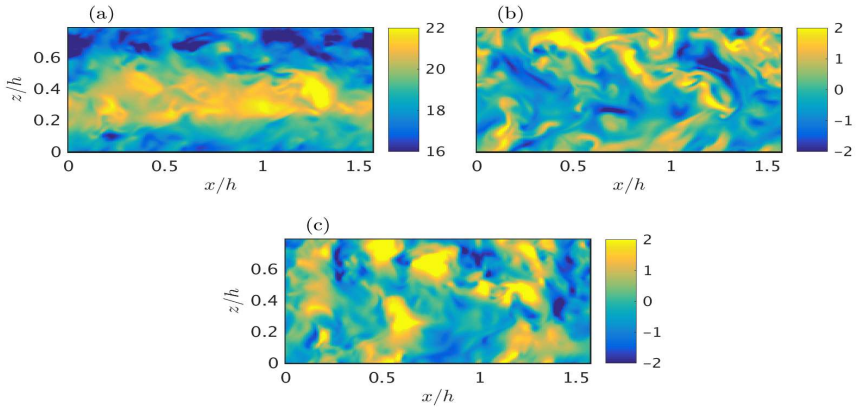

FIGURE 1. Instantaneous, (a) streamwise; (b) wall-normal; and (c) spanwise fluctuating velocities at $y = 0.25h$. Velocities in wall units.

3. Dataset

The data are obtained from direct numerical simulation of a plane turbulent channel flow with two periodic directions and no-slip condition at the wall. In the following, the streamwise, wall-normal and spanwise directions are denoted by x, y, and z, respectively, and the corresponding velocity components by u, v, and w. The friction Reynolds number of the simulation is $Re_\tau = u_\tau h/\nu = 934$, where u_τ is the friction velocity, h the channel half-height, and ν the kinematic viscosity (Pope 2000).

The incompressible Navier-Stokes equations are integrated with staggered second-order central finite differences as described in Orlandi 2000. Time advancement is achieved by a third-order Runge-Kutta scheme, combined with the fractional-step procedure. The streamwise and spanwise resolutions are $\Delta x^+ = 6.5$ and $\Delta z^+ = 3.3$, respectively, where the superscript $+$ denotes wall units defined in terms of the friction velocity and the kinematic viscosity. The minimum and maximum wall-normal resolutions are $\Delta y^+_{min} = 0.2$ and $\Delta y^+_{max} = 6.1$. The simulation was run for 140 eddy turnovers (after transients), and the velocity fields were stored every 25 wall units to build a time-resolved dataset.

The length, height and width of the computational domain are $L_x = \pi/2h$, $L_y = 2h$ and $L_z = \pi/4h$, respectively. These dimensions correspond to a minimal box simulation and are considered to be sufficient for isolating the relevant dynamical structures involved in the bursting process in the logarithmic layer (Jiménez 2012). Minimal simulation boxes have demonstrated their ability to reproduce statistics of full-size turbulence computed in much larger domains. Flores & Jiménez (2010) showed that turbulence remains "healthy" roughly below $y \approx 0.3L_z$, corresponding in our case to $y \approx 0.25h$, that is the height chosen to analyze the causality transfer between rolls and streaks in the present study.

Figure 1 shows instantaneous snapshots of the three velocity components. The streaky elongated nature of u is clearly observed along the streamwise direction, as opposed to the shorter structure of v and w. Figure 1 also highlights the finding that just a few velocity eddies are contained and isolated in the computational domain, enabling the causality analysis between individual objects.

4. Results: causal structure in the streak-roll regeneration cycle

The study of coherent structures in turbulence assumes that there is a set of coherent regions in the flow that are important enough to explain the dynamics of the flow as a whole. Of course, defining those regions is not trivial, and their relevance to the rest of the flow has to be proved. Some promising candidates are the streamwise streaks and rolls, which play an important role in near-wall turbulence production and maintenance.

The most interesting results are not the kinematic description of the structures in individual flow realizations, but rather the elucidation of how they relate to each other, and how and why they evolve in time. Such dynamical studies have been difficult in the past, and time-resolved information of three-dimensional structures has only recently become available (Lozano-Durán 2012, 2014).

In this first analysis, we define rolls as v–w motions, while streaks are characterized by low POD modes (Lumley 1967) of the streamwise velocity fluctuation, as described in the section below.

4.1. *Representation of the streaks*

POD analysis is useful in this context for efficiently representing a spatio-temporal field in terms of orthogonal modes, with energy (variance) maximized toward the lowest modes. In the present study, we perform POD analysis of the time-resolved field $u(x, h/4, z, t)$. The resulting POD modes have structures as shown in Figure 2. Due to the invariance of the solution under translations in wall-parallel planes, the modes appear in pairs with a $\pi/2$-phase difference, equivalent to the sines and cosines in the Fourier decomposition. Taking advantage of these flow symmetries, we classify the u modes into two categories, each representative of a different dynamical state of the streak. Straight modes (Figures 2(a,b)) are denoted by u_s and represent the stable configuration of the streak. Meandering modes (Figures 2(c,d,e,f)) are represented by u_m and used as surrogates for the unstable breakdown of the streaks.

4.2. *Absolute causal structure*

We investigate the causalities between the time series of the two different streak configurations, u_s and u_m, and those of v and w. Specifically, we compute the information flow rates from $u_s(x, z, t)$ and $u_m(x, z, t)$ to $v(x, z, t)$ and $w(x, z, t)$ using Eq. (2.4) at each (x, z) point. This yields a spatial distribution of causality between the corresponding u state and v or w.

Figure 3 shows the absolute information flow rates between v and the streak. The absolute causality is almost one way, i.e., from the streaks to v. And, in particular, the one-way flow is mostly between the unbroken streaks u_s and v. The meandering mode u_m is also found to be causal but weaker in strength. Note that reverse causality flows from v to the streaks exist and, though very weak, they have all passed the significance test at a 95% confidence level.

The causality between u and w (Figure 4) exhibits a different structure. As in Figure 3, the information flow rates between w and the two u states are drawn. In contrast to the previous case, u_s is barely causal with w. The information flows between u_m and w are mutual, though those from u_m still dominate.

From the previous results, we may conclude that during the streak-roll interaction, the information flow is essentially one way from the collection of unbroken streaks to v, and that the regeneration of the streaks occurs through a secondary interaction between w and u, which is mutually causal.

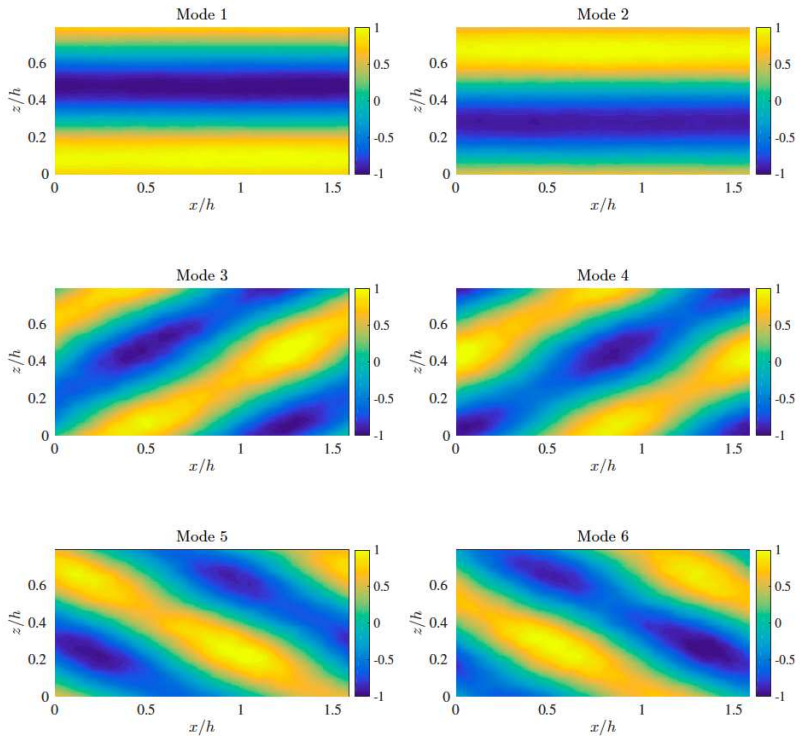

FIGURE 2. Streamwise velocity POD modes used for causal analysis.

4.3. *Normalized causal structure*

The above analysis provides the absolute information flowing between the structures. While this allows a comparison of the influences in two opposite directions, the resulting flow rates do not necessarily reflect the relative importance accounting for the formation of the structures. In some extreme cases, a tiny information flow in absolute value may turn out to dominate the entropy balance when other influences, e.g., noise, are negligible (see Liang (2015)). Considering that the rolls and streaks are on different scales, and hence their entropy balances could be quite different, it is necessary to calculate the relative or normalized causality.

Unlike that of covariance, the normalization of causality is not straightforward. Following the discussion from Section 2, the marginal entropy rate of a signal X_1 may be decomposed as (Liang 2015)

$$\frac{\mathrm{d}H_1}{\mathrm{d}t} = T_{2\to 1} + \frac{\mathrm{d}H_1^*}{\mathrm{d}t} + \frac{\mathrm{d}H_1^{\mathrm{noise}}}{\mathrm{d}t}, \tag{4.1}$$

where the first term is the transfer of entropy from signal X_2 to X_1, the second term is the self-induced change of entropy, and the third is the change due to stochastic effects. Therefore, we may choose

$$Z_{2\to 1} = |T_{2\to 1}| + \left|\frac{\mathrm{d}H_1^*}{\mathrm{d}t}\right| + \left|\frac{\mathrm{d}H_1^{\mathrm{noise}}}{\mathrm{d}t}\right| \tag{4.2}$$

as the normalizer and define $\tau_{2\to 1} = T_{2\to 1}/Z_{2\to 1}$. This way if $\tau_{2\to 1} = 1$, the variation of

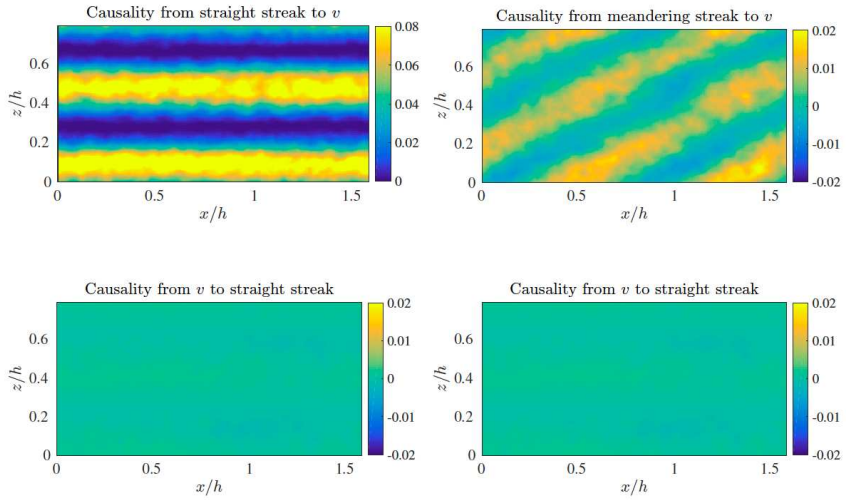

FIGURE 3. Absolute causal information flow rates (in nats per time step) between straight and meandering streaks and the wall-normal velocity.

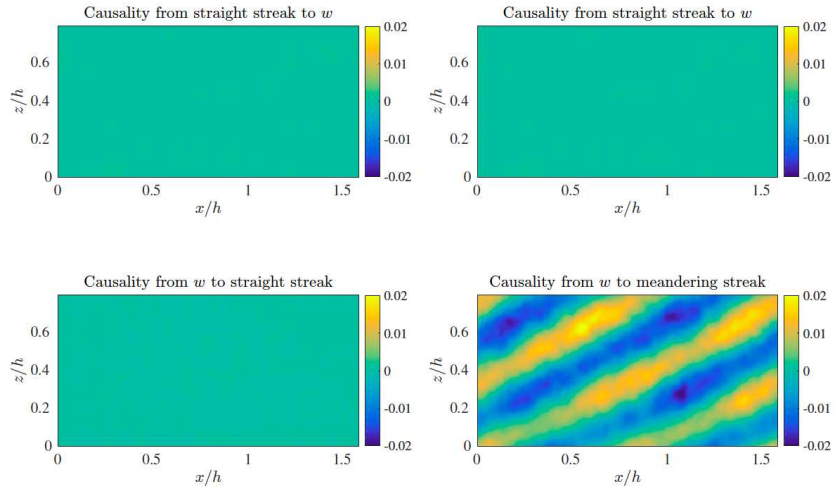

FIGURE 4. Absolute causal information flow rates (in nats per time step) between straight and meandering streaks and the spanwise velocity.

H_1 is 100% due to the information flow from X_2; if $\tau_{2\to1}$ is approximately 0, X_2 is not the cause. Therefore, $\tau_{2\to1}$ assesses the importance of the influence of X_2 on X_1 relative to other processes.

As mentioned in the preceding subsection, the absolute information flows from v to the u_s and u_m, though very weak, are actually all significant at a 95% level. When normalized, the values are significantly changed. Figure 5 shows that the relative information flow from v to the u_s dominates, reaching a percentage as high as 20%, while its reverse counterpart has a maximal value of only 10%. This is because, compared to u_s, the v field is much more disorganized, and a large fraction of its entropy balance comes from noise. So, even though the information flowing from u_s is very large, its relative weight

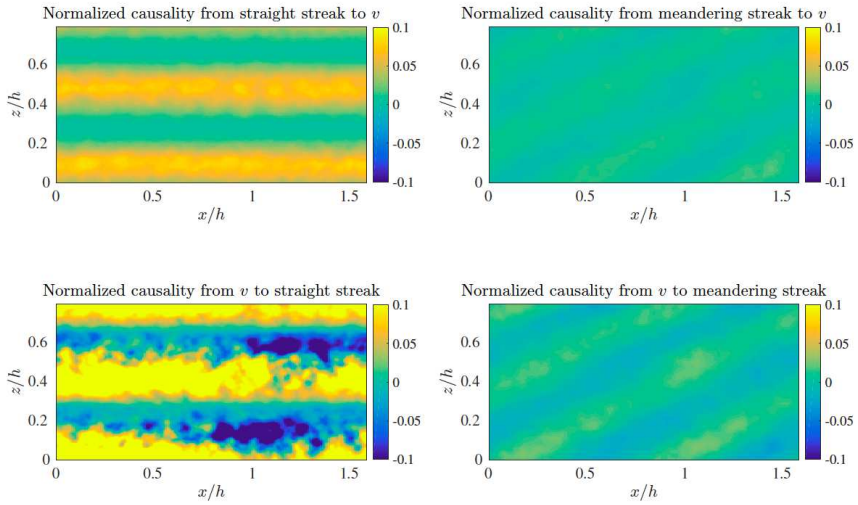

FIGURE 5. Normalized causal information flow rates between straight and meandering streaks and wall-normal velocity.

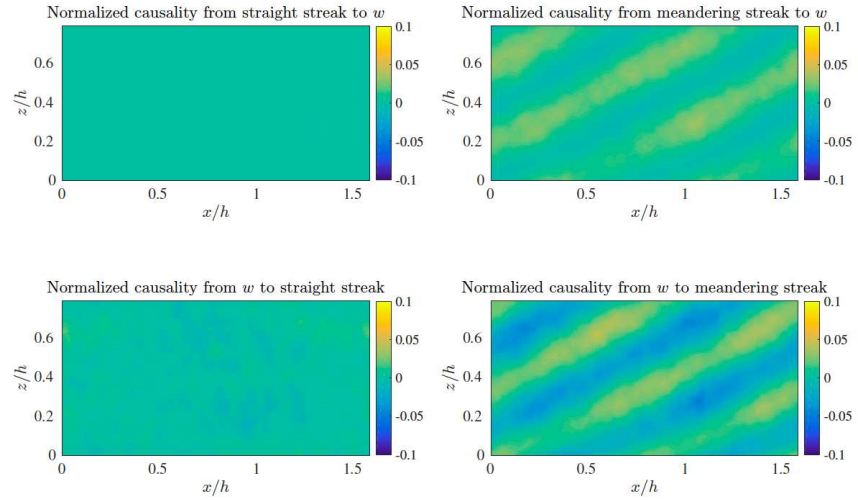

FIGURE 6. Normalized causal information flow rates between straight and meandering streaks and spanwise velocity.

is no longer relevant. In contrast, the u_s is much more coherent (less noisy), and the information flow from v, though weak, becomes significant since the signal-to-noise ratio is large.

The normalized information flows between w and u are also affected in magnitude. Though still mutually causal, the normalized flows from w become more significant, as shown in Figure 6.

In terms of normalized information flow, the conclusions are qualitatively similar to those from the previous section. The streaks and rolls are mutually causal. Specifically, the dominant causality is between the straight configuration of the streak and v, and the secondary causality between meandering streaks and w. Although not shown because of

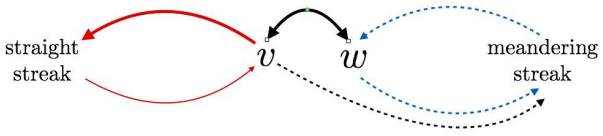

FIGURE 7. Sketch of the normalized information flow in the streak-roll regeneration cycle. Information is extracted from Figures 5 and 6, and from the normalized causal analysis between v and w (not shown). Subcycles are represented in blue and red colors. Solid and dashed arrows represent strong and weak normalized causality flows.

space restriction, the normalized causalities between the first POD modes of v and w turn out to be close to 15% in both directions. Note that the normalization of a flow from u_s to v is with respect to the entropy balance of v, which may be different from the balance of u_s, as shown above. Hence, the resulting normalized causalities cannot be compared; the comparison can be made only between absolute causalities.

5. Summary

Despite the extensive information provided by direct numerical simulation of turbulent flows, how causality emerges and is distributed has been overlooked in turbulence research. One reason may be due to the lack of appropriate research tools in the past. Recently, a rigorous and quantitative causality analysis was established for unraveling the complex causal structure and topology underlying the accumulating large datasets (Liang 2014; 2016). In this formalism, causality is measured by the rate of information flowing from one event to another. When two time series are given, the causality from one series, say X_1, to another, say X_2, can be estimated in a maximal likelihood sense. If the causality is nonzero, then X_2 is causal to X_1. A corollary is that causation implies correlation, but not vice versa.

The above formalism has been applied with remarkable success to many real-world problems. In this study, we have examined the causal structure between the streamwise rolls and streaks in the logarithmic layer of a turbulent channel flow. The proper orthogonal decomposition was first performed for the streamwise velocity u; the resulting time series for the low modes are used as surrogates for two different configurations of the streaks, that is, the straight and meandering states. Causality analysis was then conducted between these series with the time history of v and w at each spatial point, providing the distribution of information flow between the streaks at two different states and rolls.

Our results show that the streak-roll regeneration cycle may be seen as a combination of two subcycles. In the dominant subcycle, the causality flows between the straight configuration of the streak and v. The secondary interactive relation is much weaker (but still significant) and occurs between w and the meandering streak. In each subcycle the elements are mutually causal. The results are sketched in Figure 7.

In the above scenario, the most relevant interactions may be understood in the frame of simplified physical mechanisms. The causality flow from the meandering streaks to v is consistent with previous analysis where the former are most unstable to sinuous normal modal perturbations (e.g., Schoppa & Hussain 2002), while the Orr Mechanism (Orr 1907) is a reasonable candidate for the information transfer from the wall-normal velocity

to streaks in a straight configuration. The coupling between spanwise and wall-normal velocities may be anticipated by the effect of the pressure enforcing incompressibility.

It is nevertheless striking that the normalized causalities never rise above 20%, implying a strong influence of the self-induced causality and noise in the time evolution of the streaks and rolls. A more detailed causal map may be obtained by calculating the information flow as a function of time. This and other unresolved questions will be addressed in future investigations.

REFERENCES

Farrell, B.F. & Ioannou, P.J. 2012 Dynamics of streamwise rolls and streaks in turbulent wall-bounded shear flow. *J. Fluid Mech.* **708**, 149-196.

Flores, O. & Jiménez, J. 2010 Hierarchy of minimal flow units in the logarithmic layer. *Phys. Fluids* **22**, 071704.

Granger, C. 1969 Investigating causal relations by econometric models and cross-spectral methods. *Econometrica* **37**, 424.

Hamilton, K., Kim, J. & Waleffe, F. 1995 Regeneration mechanisms of near-wall turbulence structures. *J. Fluid Mech.* **287**, 317-348.

Jiménez, J. & Moin, P. 1991 The minimal flow unit in near-wall turbulence. *J. Fluid Mech.* **225**, 213-240.

Jiménez, J. & Pinelli, A. 1999 The autonomous cycle of near wall turbulence. *J. Fluid Mech.* **389**, 335-359.

Jiménez, J. 2012 Cascades in wall-bounded turbulence. *Annu. Rev. Fluid Mech.* **44**, 2-45.

Kim, J., Kline, S.J. & Reynolds, W.C. 1971 The production of turbulence near a smooth wall in a turbulent boundary layer. *J. Fluid Mech.* **50**, 133-160.

Klebanoff, P.S., Tidstrom, K.D. & Sargent, L.M. 1962 The three-dimensional nature of boundary-layer instability. *J. Fluid Mech.* **12**, 1-34.

Kline, S.J., W.C. Reynolds, Schraub, F.A., & Runstadler, P.W. 1967 Structure of turbulent boundary layers. *J. Fluid Mech.* **30**, 741-816.

Liang, X.S. 2008 Information flow within stochastic dynamical systems. *Phys. Rev. E* **78**, 031113.

Liang, X.S. 2014 Unraveling the cause-effect relation between time series. *Phys. Rev. E* **90**, 052150.

Liang, X.S. 2015 Normalizing the causality between time series. *Phys. Rev. E* **92**, 022126.

Liang, X.S. 2016 Information flow and causality as rigorous physical notions ab initio. *Phys. Rev. E* **94**, 052201.

Lozano-Durán,A. Flores,O. & Jiménez,J. The three-dimensional structure of momentum transfer in turbulent channels. *J. Fluid Mech.* **694**, 100–130.

Lozano-Durán,A. and Jiménez,J. Time-resolved evolution of coherent structures in turbulent channels: characterization of eddies and cascades. *J. Fluid Mech.* **759**, 432–471.

Lumley, J. L. 1967 The structure of inhomogeneous turbulent flows. *Atmospheric Turbulence and Radio Wave Propagation* (A. M. Yaglom & V. I. Tararsky, eds.), (Nauka, Moscow), 166-178.

Orr,W. M'F. 1907 The stability or instability of the steady motions of a perfect liquid and of a viscous liquid. Part II: A viscous liquid. *Proc. R. Ir. Acad.* **27**, 69-138.

Orlandi, P. 2000 *Fluid Flow Phenomena: A Numerical Toolkit*. Kluwer.

Pope, S.B. 2000 *Turbulent Flows*. Cambridge University Press, Cambridge, UK.

Schoppa, W. & Hussain, F. 2002 Coherent structure generation in near-wall turbulence. *J. Fluid Mech.* **453**, 57-108.

Stips, A., Macias, D., Coughlan, C., Garcia-Gorriz, E. & Liang, X.S. 2016 On the causal structure between CO_2 and global temperature. *Scientific Reports* **6**, 21691.

Tissot, G., Lozano-Durán, A., Cordier, L., Jiménez, J. & Noack, B.R. 2014 Granger causality in wall-bounded turbulence. *J. of Phys.: Conf. Series* **506**,

Waleffe, F. 1997 On a self-sustaining process in shear flows. *Phys. Fluids* **9**, 883-900.